Inorganic Chemistry

Article

pubs.acs.org/IC

Structural Phase Transitions in a New Compound Eu_2AgGe_3

Sumanta Sarkar and Sebastian C. Peter*

New Chemistry Unit, Jawaharlal Nehru Centre for Advanced Scientific Research, Jakkur, Bangalore, 560064, India

Supporting Information

ABSTRACT: A new intermetallic compound Eu_2AgGe_3 has been synthesized using high-frequency induction heating method. Single-crystal X-ray diffraction data showed that Eu_2AgGe_3 crystallizes in the orthorhombic Ba_2LiSi_3 structure type, with *Fddd* space group and lattice parameters a = 8.7069(17) Å, b = 15.011(3) Å, c = 17.761(4) Å. Eu_2AgGe_3 is composed of infinite arrays of hexagonal $[Ag_3Ge_3]$ units stacked along the [001] direction, and the Eu sites are sandwiched between these parallel hexagonal networks. Temperature-dependent powder XRD data and DTA hint toward a structural phase transition from orthorhombic to hexagonal above 477 K and an unusual reversible transition to the original phase, i.e., orthorhombic phase at around 718 K. Magnetic measurements on Eu_2AgGe_3 sample show paramagnetic behavior above 100 K and weak ferromagnetic interactions below 80 K. Mössbauer spectroscopy and X-ray absorption near-edge spectroscopic (XANES) studies reveal that Eu atoms in Eu_2AgGe_3 exist in the divalent oxidation state.

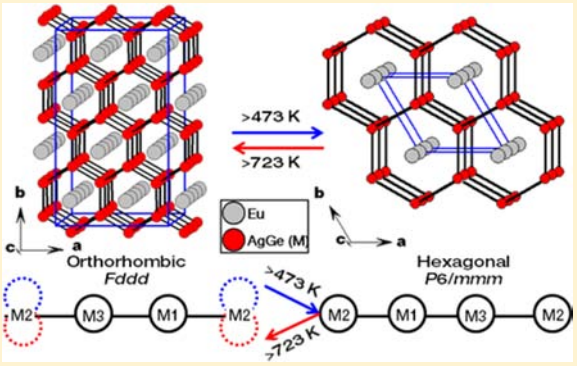

1. INTRODUCTION

Rare-earth-based intermetallic compounds show a wide range of fascinating and anomalous physical properties due to the interplay of various kinds of interactions between the localized 4f (or 5f) electrons of the rare-earth atoms and the delocalized conduction electrons.[1−4] These interactions can be modulated (or sometimes altered) by introducing chemical changes, such as doping,[5] substitution of atoms,[6] applying external pressure and/or temperature,[7] and magnetic field.[8] These modulations/alterations can also give rise to diverse crystal structures (sometimes new structures) and phase transitions in these types of compounds.

In this context, it should be mentioned that many of the compounds with general formula RE_2TX_3 (where, RE = lanthanide and actinides; T = transition metal series; X = p-block elements) are ordered superstructures of the AlB_2 structure type and have been studied extensively for last two decades for their structural diversity and interesting physical properties.[9−18] Hoffmann et al.[9] discussed the group−subgroup relations in the AlB_2 family on the basis of the Bärnighausen formalism.[19,20] The ordering of the transition metal atoms and main group elements at the boron positions in the planar hexagonal ring of AlB_2 type may result in loss of the basic hexagonal symmetry, as described by Hoffmann et al.[9] Depending on the extent of tilting and distortions of the hexagonal rings, these compounds may crystallize in the hexagonal, orthorhombic, and monoclinic structures. There are numerous compounds reported[9,21−24] in the RE_2TX_3 family crystallizing in various superstructures of the AlB_2 type. The dimension of the supercell and puckering of the hexagonal network occur depending on the size of the atoms, valence electron count (VEC), and nature of bonding (i.e., extent of ionicity, aromaticity in the hexagonal ring, etc.).

Rare-earth (RE) elements occupying the aluminum site also play a crucial role in tilting and distorting the hexagons, especially when they can exhibit valence fluctuations or mixed valence behaviors. Ce, Eu, and Yb are of particular interest in this regard. These three elements can show variable valencies, $Ce^{3+/4+}$, $Eu^{2+/3+}$, and $Yb^{2+/3+}$,[25] which may give rise to many interesting properties like heavy fermion behavior,[26,27] Kondo effect,[28−30] valence fluctuation, as well as structural transition.[26,27,31−37]

Motivated by the fact that Au forms a stable phase with Eu in the RE_2TGe_3 family.[37] we anticipated that Ag might be a valid candidate to form the same phase; indeed, we discovered a new compound Eu_2AgGe_3 using high-frequency induction heating method. Here, we report the crystal structure of Eu_2AgGe_3 using X-ray diffraction on single crystals. Temperature-dependent powder XRD and DTA reveal reversible phase transitions which are rare in intermetallics, and we explained this using a displacive transition mechanism of the Ag and Ge atoms at the hexagonal rings. Magnetic measurements, X-ray absorption near-edge spectroscopy (XANES), and Mössbauer spectroscopy on Eu_2AgGe_3 showed that Eu atoms are in the divalent state.

2. EXPERIMENTAL SECTION

2.1. Synthesis. The following reagents were used as purchased without further purification: Eu (ingots 99.99%, ESPI metals), Ag (ingots, 99.99%, Alfa-Aesar), and Ge (metal pieces 99.999%, Alfa Aesar). Europium, silver, and germanium metals were taken in ideal

Received: February 12, 2013
Published: August 21, 2013

   dx.doi.org/10.1021/ic400369a | Inorg. Chem. 2013, 52, 9741−9748

2:1:3 atomic ratios and sealed in tantalum ampules in an arc-melting apparatus (Edmund Bïühler Gmbh, compact arc melter MAM-1) under argon atmosphere. The sealed tantalum ampules were then placed in a water-cooled sample chamber of an induction furnace (EasyHeat induction heating system, model 7590), first rapidly heated to ca. 1250 K and kept at that temperature for 10 min. Then the sample was cooled to ca. 1000 K, and the sample was annealed at that temperature for another 30 min, followed by quenching by switching off the power supply. The brittle product with metallic luster could easily be separated from the tantalum tube. No reaction with the container was observed up to the detection limit of powder X-ray diffraction. The compound is stable in air for several months. Irregular-shaped single crystals were hand picked under a laboratory microscope and used for X-ray diffraction studies. The same batch was used for all other characterization and physical property studies.

Our previous work on crystal growth of Eu_2AuGe_3 and Yb_2AuGe_3 using metal flux techniques in excess indium[36,37] motivated us to synthesize Eu_2AgGe_3 in indium and gallium flux with different temperature profiles and different initial element stoichiometry, but our attempts were unsuccessful perhaps due to the low diffusion rate or immiscibility of Ag. In all cases, unreacted Ag and Ge were found in the sample and $EuGe_2$ was obtained as the major phase.

2.2. Powder X-ray Diffraction. The phase identity and purity of the Eu_2AgGe_3 compound were confirmed by powder XRD experiments carried out with a Bruker D8 Discover diffractometer using Cu Kα radiation (λ = 1.54187 Å). The experimental powder pattern of Eu_2AgGe_3 was compared to the pattern simulated from single-crystal X-ray structure refinement within the *Fddd* space group and found to be in good agreement. The stronger reflections could easily be indexed on the basis of the orthorhombic unit cell, Ca_2AgSi_3 structure type, *Fmmm* space group. When weak reflections (shown in Supporting Information, Figure S1) observed in the powder diffraction pattern were included, refinement resulted in the superstructure of Eu_2AgGe_3, Ba_2LiSi_3 structure type (*Fddd* space group) with lattice parameters of a = 8.7069(17) Å, b = 15.011(3) Å, and c = 17.761(4) Å.

Powder XRD data were collected in the temperature range 303–973 K using the same instrument under vacuum condition (10^{-6} Torr pressure) on a platinum plate.

2.3. Differential Thermal Analysis. Differential thermal analysis (DTA) was performed using a differential scanning calorimeter (METTLER-TOLEDO DSC1) at the Indian Institute of Science, Bangalore facility. The sample (19.56 mg) was taken in an alumina crucible and heated from 303 to 823 K at a rate of 5 K/min in an inert N_2 atmosphere followed by cooling at the same rate to 303 K.

2.4. Single-Crystal X-ray Diffraction. A carefully selected single crystal of Eu_2AgGe_3 was mounted on a thin glass fiber. X-ray single-crystal structural data of Eu_2AgGe_3 were collected on a STOE IPDS 2T diffractometer with graphite monochromatic Mo Kα radiation (λ = 0.71073 Å) operating at 50 kV and 30 mA. The X-AREA (X-RED and X-SHAPE within)[38] package suite was used for data extraction, integration and to apply numerical absorption corrections. The structure was solved by SHELXS 97[39] and refined by a full matrix least-squares method using SHELXL.[40] The compound was found to crystallize in *Fddd* space group with lattice parameters a = 8.7069(17) Å, b = 15.011(3) Å, c = 17.761(4) Å. The model obtained from refinement using the *Fddd* space group was used for Rietveld refinement of the PXRD data using the program FullProf.[41] Fitting was quite satisfactory with a chi squared value of 3.16 (Figure S2, Supporting Information), whereas the strong substructure peaks matched very well with the simulated data obtained from *P6/mmm* space group with hexagonal structure (Figure S3, Supporting Information).

2.5. Structure Refinement. Single-crystal data of Eu_2AgGe_3 showed an orthorhombic cell. The lattice was established as face-centered orthorhombic based on absences of odd $h + k$, $h + l$, and $k + l$ reflections and compatible with space groups *Fmmm*, *Fmm*2, and *F*222. In the first refinement step, all weak superstructure reflections have been neglected and only the subcell intensities have been integrated with lattice parameters a = 8.7069(17) Å, b = 15.011(3) Å, and c = 8.8803(18) Å. Since the powder XRD of Eu_2AgGe_3 is similar to the pattern of Eu_2AuGe_3[37] and Yb_2AuGe_3[36] compounds (Ca_2AgSi_3 type,[9] space group *Fmmm*), the atomic coordinates of Eu_2AuGe_3 were taken as starting values and the structure was refined with anisotropic displacement parameters for all atoms with SHELXL-97 (full-matrix least-squares on F_o^2).[40] As a check for the correct composition, the occupancy parameters were refined in a separate series of least-squares cycles. Initially, there were five crystallographically different positions in the Eu_2AgGe_3 compound: two for each Eu and Ge atom and one for the Ag atom. During isotropic refinement it was observed that the anisotropic displacement parameters of the silver and germanium atoms were anomalously large. Furthermore, refinement was largely unsatisfactory, giving relatively high residuals (R_1 > 10%) and large electron density residuals (15–20 e Å^{-3}) around the silver and germanium atoms. Anisotropic refinement did not improve these parameters and also resulted in abnormal cigar-shaped silver and germanium thermal ellipsoids (U_{22} = 0.080 Å^2). Similar problems were also faced while refining the crystal structure of the Yb_2AuGe_3 compound as well.[36] The anomalous thermal parameter could not be resolved by subsequent refinement of the occupancy parameters. All these observations indicated a crystallographic disorder associated with the Ge and Ag atoms similar to the Yb_2AuGe_3 compound. Consequently, refinement was performed by allowing mixed Ag/Ge occupancy of both the "Ge" and the "Ag" positions, subject to the constraint that the summed occupancies of both sites were full. This makes the compound slightly off different stoichiometry. At this point, it must be mentioned that mixing of silver and germanium was also reported in the equiatomic compound EuAgGe.[42,43] Though the residual R_1 reduced substantially to 5.6% and electron density residuals are behaving properly (2.9 and −1.8 e Å^{-3}), the thermal ellipsoid U_{22} for M3 (Ge3 + Ag3) atoms was significantly larger (0.064 Å^2). Nevertheless, when we attempted to remove the mirror plane along the c axis and refine the crystal structure in *Fmm*2 space group, larger residuals and thermal displacement parameters resulted. *F*222 is another space group used, but all refinement parameters were similar to refinement in the *Fmmm* space group.

The weak superstructure reflections observed in the PXRD (shown in the Supporting Information, Figure S1) have been considered in the second step. Additional reflections suggested doubling of the c axis and resulted in lattice parameters a = 8.7069(17) Å, b = 15.011(3) Å, and c = 17.761(4) Å. Superstructure reflections were already evident from the powder X-ray diffraction data and indicate that the structure is compatible with the Ba_2LiSi_3-type structure. Atomic parameters of Ba_2LiSi_3 were taken as starting parameters, and the structure was refined using SHELXL-97 (full-matrix least-squares on F^2)[40] with anisotropic atomic displacement parameters for all atoms. Refinement within the Ba_2LiSi_3-type structure also resulted with 5 atomic positions: two europium atoms and three mixed position of silver and germanium. Resulting anisotropic displacement parameters of mixed position became well behaved, and final difference maps showed residuals that were reasonably acceptable. Owing to many weak reflections and doubling of the unit cell, the quality of the refinement did not satisfy criteria of a high-quality structure refinement. Relatively large displacement parameters of *M*2 and *M*3 positions (i.e., along the c axis) indicated a further symmetry reduction at low temperature similar to our previous report on Eu_2AuGe_3.[37] Final refinement gives an atomic ratio of $Eu_2Ag_{1.21(2)}Ge_{2.79(2)}$. Data collection and refinement parameters are summarized in Table 1. Atomic coordinates, equivalent displacement parameters, anisotropic displacement parameters, and important bond lengths are listed in Tables S1, S2, and S3, respectively (Supporting Information).

2.6. Elemental Analysis. Semiquantitative microanalyses were performed on the irregular-shaped single crystals obtained from the ingots after induction furnace heating using a scanning Leica 220i electron microscope equipped with a Bruker 129 eV energy-dispersive X-ray analyzer. Data were acquired using standardless analysis with an accelerating voltage of 20 kV and in 90 s accumulation time. EDS analyses taken on visibly clean surfaces of Eu_2AgGe_3 crystals gave an atomic composition of 32(±1)% Eu, 20(±1)% Ag, and 46(±2)% Ge, which is in good agreement with the composition obtained from the single-crystal X-ray diffraction data. No traces of Ta (from the

dx.doi.org/10.1021/ic400369a | Inorg. Chem. 2013, 52, 9741–9748

Table 1. Crystal Data and Structure Refinement for Eu_2AgGe_3 at 293(2) K[a]

fw	636.22	636.22
wavelength	0.71073 Å	0.71073 Å
cryst syst	orthorhombic	orthorhombic
space group	*Fmmm*	*Fddd*
unit cell dimens	a = 8.7069(17) Å	a = 8.7069(17) Å
	b = 15.011(3) Å	b = 15.011(3) Å
	c = 8.8803(18) Å	c = 17.761(4) Å
volume	1160.66(4) Å^3	2321.33(8) Å^3
Z	8	16
density (calcd)	7.282 g/cm^3	7.296 g/cm^3
abs coeff	39.427 mm^{-1}	39.319 mm^{-1}
F(000)	2181	4362
cryst size	0.12 × 0.10 × 0.08 mm^3	0.12 × 0.10 × 0.08 mm^3
θ range for data collection	2.71−29.16°	2.9−29.14°
index ranges	$-11 \le h \le 11$, $-12 \le k \le 11$, $-18 \le l \le 20$	$-11 \le h \le 11$, $-20 \le k \le 20$, $-24 \le l \le 23$
no. of reflns collected	2671	4583
no. of independent reflns	445 [R_{int} = 0.0906]	769 [R_{int} = 0.0921]
completeness to θ = 34.26°	98.0%	98.1%
refinement method	full-matrix least-squares on F^2	full-matrix least-squares on F^2
data/restraints/params	353/0/26	769/0/34
goodness-of-fit	1.274	1.424
final R indices [$>2\sigma$(I)]	R_{obs} = 0.0560, wR_{obs} = 0.1602	R_{obs} = 0.0769, wR_{obs} = 0.1720
R indices [all data]	R_{all} = 0.0649, wR_{all} = 0.1564	R_{all} = 0.0909, wR_{all} = 0.179
extinction coefficient	0.00052(11)	0.000125(2)
largest diff. peak and hole	2.923 and −1.851 e·Å^{-3}	2.442 and −1.655 e·Å^{-3}

[a] $R = \Sigma||F_o| - |F_c||/\Sigma|F_o|$, $wR = \{\Sigma[w(|F_o|^2 - |F_c|^2)^2]/\Sigma[w(|F_o|^4)]\}^{1/2}$, and calcd $w = 1/[\sigma^2(F_o^2) + (0.0306P)^2 + 142.9431P]$, where $P = (F_o^2 + 2F_c^2)/3$.

crucible) were found in the data. The EDS spectrum is shown in Figure S4, Supporting Information.

2.7. Magnetic Measurements. Magnetic measurements on powder samples of Eu_2AgGe_3 were carried out with a Quantum Design Magnetic Property Measurement System, Superconducting Quantum Interference Device (MPMS-SQUID) dc magnetometer. Temperature-dependent magnetization data were collected in the field-cooled mode (FC) in a temperature range from 2 to 300 K at an applied magnetic field of 1000 Oe. Magnetization data were also collected for Eu_2AgGe_3 at three different temperatures, viz. 5, 18, and 300 K, with field sweeping from −55 to 55 kOe (Figure S5, Supporting Information).

2.8. X-ray Absorption Near-Edge Spectroscopy (XANES). X-ray absorption near-edge spectroscopy (XANES) experiments were performed at PETRA III, P06 beamline of DESY, Germany. Measurements at the Eu L_{III} edge and ambient pressure were performed in transmission mode using gas ionization chambers to monitor the incident and transmitted X-ray intensities. Monochromatic X-rays were obtained using a Si(111) double-crystal monochromator which was calibrated by defining the inflection point (first derivative maxima) of Cu foil as 8980.5 eV. The beam was focused employing a Kirkpatrick−Baez (K−B) mirror optic. A rhodium-coated X-ray mirror was utilized to suppress higher order harmonics. A CCD detector was used to record the transmitted signals. Sample was prepared by mixing an appropriate amount of finely ground powder with cellulose and cold pressing them to a pellet.

2.9. ^{151}Eu Mössbauer Spectroscopy. ^{151}Eu Mössbauer measurements were carried out in the transmission geometry using a standard PC-based spectrometer in the temperature range of 30−300 K using $^{151}SmF_3$ as the source in the experiment and Eu_2O_3 as the reference sample.

3. RESULTS AND DISCUSSION

3.1. Crystal Structure. The crystal structure of Eu_2AgGe_3 along the b and c axes is shown in Figure 1. Eu_2AgGe_3 crystallizes in the Ba_2LiSi_3 structure type, an ordered superstructure of the hexagonal AlB_2 type with *Fddd* space group, and lattice parameters are a = 8.7069(17) Å, b = 15.011(3) Å, and c = 17.761(4) Å.

In analogy to Ba_2LiSi_3 and other related compounds, the crystal structure of Eu_2AgGe_3 can also be described as a "filled variation" of orthorhombic β-K_4P_6 structure,[44] which is another symmetry-reduced variant of the AlB_2 prototype. The crystal structure of Eu_2AgGe_3 consists of an infinitely extended hexagonal network of three nonequivalent crystallographic sites, namely, M1, M2, and M3, all of them are the mixed positions of Ag and Ge atoms with varied occupancy levels (Table 1).[42,43] These layers are stacked parallel along the [001] direction (considering the c axis as the pseudohexagonal axis) with two crystallographically different Eu atoms sandwiched

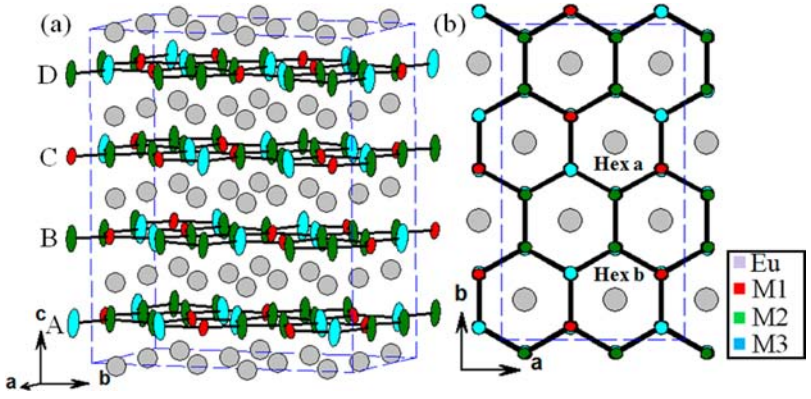

Figure 1. Crystal structures of Eu_2AgGe_3 in *Fddd* space group viewed approximately along (a) [100] and (b) [001] directions are shown here in the ellipsoid model (Eu sites are kept in spherical model for the sake of simplicity). Unit cell is marked by dashed blue lines. Three different [AgGe] mixed sites (marked by M1, M2, and M3) are shown in three different color codes. Hexagonal layers are stacked along the c axis in ABCD, ABCD sequence. Two hexagons (Hex a and b) are joined by M2 sites along the [010] direction.

dx.doi.org/10.1021/ic400369a | *Inorg. Chem.* 2013, 52, 9741−9748

between these layers. At this point, it is worthwhile to compare the crystallographic features of Eu_2AgGe_3 (Ba_2LiSi_3 structure type) and Eu_2AuGe_3 (Ca_2AgSi_3 structure type). Hexagonal rings in Eu_2AgGe_3 are slightly more puckered owing to the higher degree of ordering between Ag and Ge in comparison to Au and Ge in Eu_2AuGe_3 (*Fmmm*), which has basically planar [Ge_6] and [Au_2Ge_4] hexagons. Layers consisting of Eu atoms are also distorted, and they align in a zigzag fashion which we assume is an effect of puckering in the hexagonal ring.[12] Hexagonal layers in Eu_2AgGe_3 are stacked in the sequence ABCD, ABCD along the [001] axis, whereas for Eu_2AuGe_3 the stacking sequence of the hexagonal layers is AB, AB along the same axis. Another noticeable difference lies in the ordering of the transition metal and Ge atoms in the hexagonal network itself. In Eu_2AuGe_3 the [Ge_6] and [Au_2Ge_4] hexagons are linked by Au atoms with no mixed sites between Au and Ge positions; on the contrary, all positions in the hexagonal network in Eu_2AgGe_3 consist of Ag and Ge mixed sites.

The distance between two parallel hexagonal layers is in the range 4.3699−4.5396 Å. The intralayer distance between two adjacent Eu atoms ranges from 4.3086 to 4.3129 Å and are slightly shorter than the interlayer distances 4.4135−4.4689 Å. These values suggest the possible presence of divalent Eu atoms in Eu_2AgGe_3 as they are close to the values in other already reported intermetallic compounds consisting of purely divalent Eu, such as Eu_2AuGe_3,[37] $EuCu_2Si_2$,[45,46] $EuGe_2$,[47] etc., whereas the Eu−Eu distance in $EuPd_3$ with purely trivalent Eu is 4.10 Å,[48] which is comparatively smaller than the values observed in divalent Eu-containing intermetallics. Later, these observations were confirmed by magnetic, XANES, and Mössbauer spectroscopic studies. The smallest bond distances between different mixed positions within the hexagonal network are 2.5618(16), 2.547(3), and 2.4596(18) Å for M1−M2, M1−M3, and M2−M3, respectively. The first two bond distances are very close to the sum of the covalent radii of Ag and Ge (2.56 Å),[49] whereas the last one is similar to the Ge−Ge bond distance (2.45 Å) in elemental Ge,[50] indicating almost negligible bonding contribution from the Ag atom for M3. A further band structure calculation study will help to understand the role of bonding (both σ and π electrons) features in the hexagonal network toward superstructure formation in this compound.

The coordination environments of Eu1, Eu2, and the [Ag + Ge] mixed sites are shown in Figure 2. Both Eu sites are in a slightly distorted hexagonal prismatic coordination environment built up by 12 [AgGe] mixed sites. Each Eu atom has eight nearest Eu neighbors: a hexagonal arrangement of six Eu atoms along with two other Eu atoms perpendicular to this plane. The [AgGe] mixed sites have tricapped trigonal prismatic coordination. The trigonal prism consists of six Eu atoms with the three faces capped with three [AgGe] mixed sites (M_3Eu_6). Though both Eu1 and Eu2 reside in a similar coordination environment, the distances between Eu1−M1/M2/M3 (3.3527(9), 3.2716(18), and 3.3081(19) Å, respectively) are slightly different from Eu2−M1/M2/M3 (3.3393(14), 3.3275(18), and 3.3759(11) Å, respectively). This kind of versatility in bond distances can directly affect the hybridization between the rare-earth f orbital and the d orbital of the transition metal and in turn may give rise to anomalies in the magnetic and electronic properties of the intermetallic compound.[51,52]

Finally, we compare Eu_2AgGe_3 with the equiatomic compound EuAgGe (*P6/mmm*).[53] Though both compounds

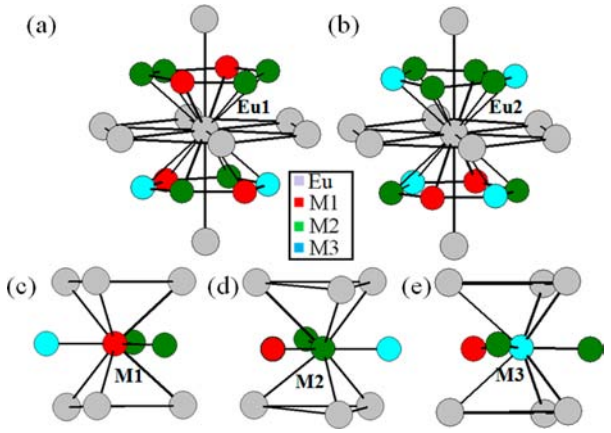

Figure 2. Coordination environment of different atoms: (a) pseudo-Frank−Kasper-type coordination for Eu1; (b) pseudo-Frank−Kasper-type coordination for Eu2; (c) tricapped trigonal prism-type coordination for the mixed positions of Ag and Ge atoms.

contain [Ag + Ge] mixed sites, the former is comprised of puckered hexagonal rings whereas the latter contains completely flat rings. This hints toward the fact that d^{10}−d^{10} interactions (which are considered to be important for puckering of hexagonal rings)[37] between the interlayer Ag atoms are dissimilar in these two compounds. Hence, with an increase in Ge content from EuAgGe to Eu_2AgGe_3, d^{10}−d^{10} (if any) is somewhat modulated.

3.2. Reversible Phase Transition. One can anticipate that the puckered hexagonal rings and valence instability of Eu atoms can influence the structural phase transition in these compounds. In order to find this, we performed temperature-dependent powder XRD. A comparison of powder XRD patterns at temperatures of 303, 523, 723, and 773 K is shown in Figure 3. The initial (303 K) pattern corresponds to the

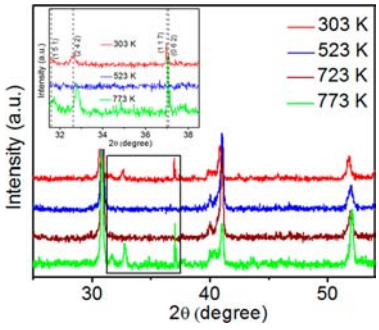

Figure 3. Temperature-dependent powder XRD pattern measured at 303, 523, 723, and 773 K. (Inset) Expanded ranges of the superstructure peaks observed in the orthorhombic crystal structure and *hkl* of four superstructure peaks are marked.

orthorhombic superstructure of Eu_2AgGe_3 (*Fddd* space group) followed by a phase transition to a higher symmetrical hexagonal above 473 K, which was stable up to 723 K. The initial orthorhombic phase reappears at 773 K, which is unusual as with an enhancement in temperature the symmetry of the system is supposed to be increased. To further prove the hexagonal symmetry, the orthorhombic superstructure reflections were removed in the single-crystal data and refined the structure in the hexagonal *P6/mmm* space group (cif file in the Supporting Information). Our simulated PXRD pattern from

dx.doi.org/10.1021/ic400369a | *Inorg. Chem.* 2013, 52, 9741−9748

the refinement data in hexagonal space group is in good agreement with the data collected above 477 K and below 723 K (Figure S3, Supporting Information).

Later, differential thermal analysis (DTA) was performed on the powdered sample of Eu_2AgGe_3 to ascertain the occurrence and exact transition temperature of the phase transitions as observed in the temperature-dependent PXRD data. The change in heat flow (in W/g unit) against temperature during the heating and cooling processes is shown in Figure 4. The

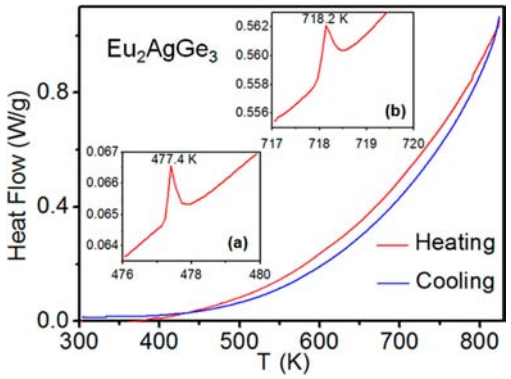

Figure 4. Differential scanning calorimetric analysis data plotted as heat change vs temperature in both heating and cooling mode. (Inset a) First transition at 477 K, and (inset b) second broad transition at 718 K.

heating curve shows two consecutive phase transitions at 477 and 718 K: the first one corresponds to orthorhombic to hexagonal phase and the second one is from hexagonal to orthorhombic phase as observed from the temperature-dependent powdered XRD data (shown as an inset of Figure 4), whereas there is no hint of other phase transitions during the cooling process, indicating that the second phase (orthorhombic) at higher temperature was stable and irreversible in nature.

We propose a displacive transition mechanism (Figure 5) for this unusual reversible phase transition observed in temperature-dependent XRD and DTA studies. At 303 K the hexagonal rings, which are made up of Ag and Ge atoms, are puckered as boat shaped and resulted in the orthorhombic crystal system. The extent of puckering is much more at the M2 site (32*h* Wyckoff site) compared to other atoms and remained above and below the plane. The two adjacent boat-shaped hexagonal rings (Hex-a and Hex-b) are joined by M2−M2 bonds. At higher temperature (above 473 K), the M2 atoms move alternatively up and down along the *c* axis and the hexagonal rings become flattened, giving rise to planar hexagonal rings. Though the thermal ellipsoids along the *c* axis (U_{33}) for M2 and M3 are reasonably large and similar in the *Fddd* refinement (0.043(2) and 0.049(2) Å^2, respectively), the higher U_{33} value of M2 in *Fmmm* (0.065(2) Å^2) compared to M3 (0.033(2) Å^2) suggests that M2 sites are more unstable compared to M3. It was also noticed that M2−M2 bonds (2.46 Å) are comparatively more strained than M2−M3 bonds (2.56 Å). This gives an additional indication that the displacive mechanism majorly involves movement of M2 sites along the *c* axis, keeping M1 and M3 sites intact at their positions. This resulted in addition of symmetries and transformed into a more symmetrical hexagonal system (AlB_2 structure type and *P6/mmm* space group). As the temperature increased further, the alternate M2 positions move further opposite to each other

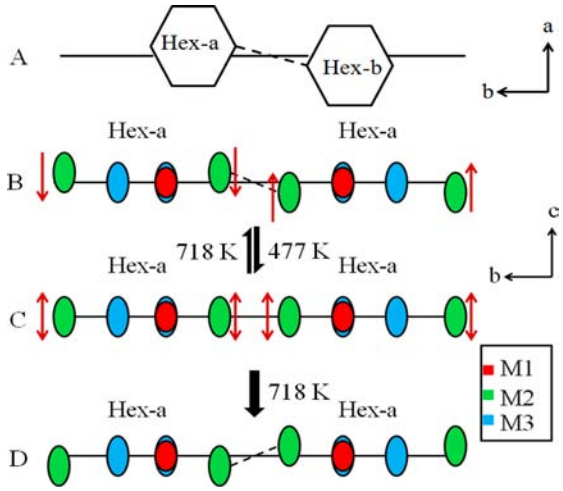

Figure 5. Schematic representation of the temperature-dependent displacive mechanism for the reversible phase transition in Eu_2AgGe_3. (A) Two hexagon rings in the orthorhombic structure of Eu_2AgGe_3 are viewed along the *c* axis. (B) Cartoon representation of these two hexagon rings along the *a* axis is shown with a probability of 90% ellipsoid atomic model. Up and down motion of two adjacent hexagonal rings through the M2−M2 bond along the *c* axis at 303 K (B), between 477 and 718 K (C), and above 718 K (D) are marked as red arrows. Tilting of the two rings is marked as dashed lines between the M2 atoms.

along the *c* direction or go back to the original positions as shown in Figure 5D/5B, resulting in another puckered arrangement of the hexagonal rings which gives rise to second phase transition around 723 K corresponding to the initial orthorhombic phase. This kind of reversible displacive phase transition was never reported in the family of intermetallics; nevertheless, it was reported in Ti−Ni-based binary[54,55] as well as ternary alloy such as $Ti_{50}Ni_{40}Cu$ (ref 56 and references therein).

3.3. Magnetic Properties. The temperature-dependent molar magnetic susceptibility of a polycrystalline sample of Eu_2AgGe_3 at an applied field of 1 kOe is shown in Figure 6. The inverse susceptibility (χ^{-1}) is plotted as a function of temperature, shown in Figure 6. The inverse susceptibility curve obeys a modified Curie−Weiss law, $\chi = C/(T - \theta_p)$, above 80 K and deviates from linearity below this temperature.

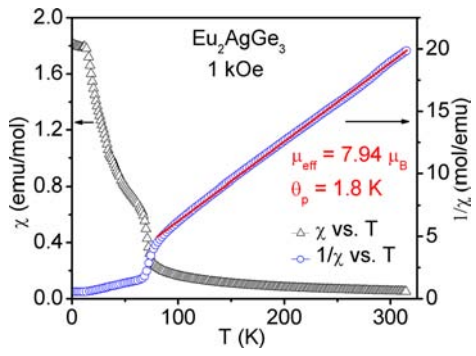

Figure 6. Temperature dependence of the molar magnetic susceptibility of Eu_2AgGe_3 at 1000 Oe applied magnetic field plotted against the *X* axis on the left-hand side. Plot on the right-hand side shows the temperature dependence of the molar inverse magnetic susceptibility of Eu_2AgGe_3, and solid red line is the Curie−Weiss fitting in the temperature range 80−325 K.

dx.doi.org/10.1021/ic400369a | Inorg. Chem. 2013, 52, 9741−9748

A linear fit with the Curie−Weiss law in the temperature range of 80−325 K gives a value of the paramagnetic Curie temperature (θ_p) of 1.8 K and an effective magnetic moment (μ_{eff}) of 7.94 μ_B/Eu ion. The positive sign of θ_p indicates an overall ferromagnetic interaction between adjacent Eu centers, but the extent of this interaction is very low as evident from the low value of θ_p. The calculated effective magnetic moment/Eu is exactly the same as the spin-only value for a divalent Eu (7.94 μ_B) in the higher temperature range (80−325 K). This is also supported by the adjacent Eu−Eu distance (4.3086−4.5396 Å) as already discussed in the Crystal Structure section.

3.4. Valence State of Europium. X-ray absorption near-edge spectroscopy (XANES) is a strong experimental tool in order to firmly establish the valence state of an element in a compound. This prompted us to investigate the Eu valence state by XANES at the Eu L_{III} edge. A sharp signal at 6973 eV was observed in the Eu-L_{III} X-ray absorption spectrum of Eu_2AgGe_3 (Figure 7). This value is characteristic of the $4f^7$

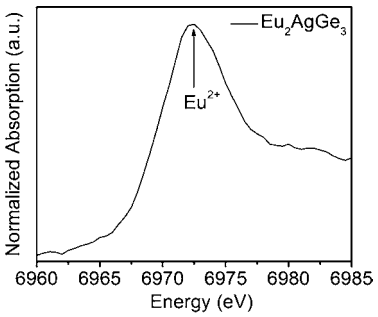

Figure 7. Eu L_{III} absorption edge spectra of Eu in Eu_2AgGe_3 at 300 K.

(Eu^{2+}) configuration and arises due to a $2p_{3/2}$ to 5d transition.[57,58] The main signal observed for the reference Eu_2O_3 (electronic configuration $4f^6$, Eu^{3+}) is approximately located around 6984 eV.[59,60] The absence of any broad shoulder around this value eliminates the possibility of mixed or intermediate valency for Eu, and thus, Eu_2AgGe_3 solely contains Eu^{2+} as an active valence state.

To further support the magnetic susceptibility and XANES data and get an idea about the local environment of the Eu atoms in our compound, we performed ^{151}Eu Mössbauer spectroscopy on Eu_2AgGe_3 samples at 30, 50, 100, and 300 K (Figure 8). Data was fitted using a Lorentzian model (area equal method),[61] and fitting parameters are given in Table 2. The average isomer shift at 303 K in Eu_2AgGe_3 (−10.34 mms^{-1}) is slightly higher than Eu_2AuGe_3 (−10.93 mms^{-1}) and EuAgGe (−10.63 mms^{-1}),[61] indicating slightly lower iconicity (i.e., higher s electron density). At all measured temperatures the spectra had a single signal around −10 mm/s, indicating the presence of pure divalent Eu, further confirming the magnetic measurements data. A fit to this signal shows the presence of two equivalent Eu^{2+} atoms in a 1:1 ratio, clearly confirming our crystallographic studies. A slightly higher experimental line width (2.67 mms^{-1}) compared to the typical value of 2.3 mms^{-1} can be explained on the basis of the presence of two crystallographically different Eu sites showing superposition in the experimental spectrum.[37] At this point it is worthwhile to mention that the isomer shift values for Eu1 and Eu2 are not the same, which corroborate with the different coordination environment of Eu atoms observed in the crystal structure

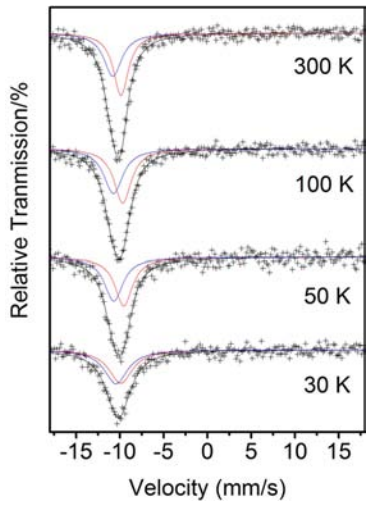

Figure 8. Experimental and simulated ^{151}Eu Mössbauer spectra of Eu_2AgGe_3 in the temperature range 30−300 K.

Table 2. Fitting Parameters of ^{151}Eu Mossbauer Spectroscopic Measurements of Eu_2AgGe_3

temp (K)	isomer shift (mm/s)	fwhm (mm/s)	area (%)	χ^2
300	−10.8 ± 0.06	2.47 ± 0.17	50	0.80
	−9.87 ± 0.05	2.06 ± 0.08	50	
100	−10.74 ± 0.05	2.63 ± 0.14	50	1.09
	−9.68 ± 0.05	2.39 ± 0.10	50	
50	−10.44 ± 0.30	3.20 ± 0.54	50	0.89
	−9.56 ± 0.07	2.39 ± 0.16	50	
30	−10.8 ± 0.06	2.47 ± 0.17	50	0.90
	−9.90 ± 0.31	3.22 ± 0.45	50	

obtained from single-crystal XRD and also suggests that the local electronic density around Eu1 and Eu2 is different.

4. CONCLUDING REMARKS

A new compound, Eu_2AgGe_3 has been discovered in the family of AlB_2 type. Due to the different puckering behavior of the Ag_3Ge_3 layer, Eu_2AgGe_3 crystallizes in the Ba_2LiSi_3 structure type with *Fddd* space group. Temperature-dependent PXRD suggest a reversible crystal structure transition which was very well supported by DTA. Eu_2AgGe_3 is in fact the first intermetallic compound that shows reversible phase transitions, which have been explained by the displacive transition mechanism of Ag and Ge atoms in the hexagon layers. Our observations open up the possibility to study the phase transition in all compounds crystallizing in the AlB_2 family. A rare high-temperature reversible structural transition in Eu_2AgGe_3 will be interesting for researchers to study in the field of material chemistry and condensed matter physics.

■ ASSOCIATED CONTENT

Supporting Information

Crystallographic information files (CIF), tables for atomic coordinates, isotropic displacement and anisotropic displacement parameters, and bond lengths; Rietveld refinement of X-ray powder diffraction pattern and powder XRD comparison plots for substructure and superstructure and *M* vs *H* plots at different temperatures. This material is available free of charge via the Internet at http://pubs.acs.org.

dx.doi.org/10.1021/ic400369a | *Inorg. Chem.* 2013, 52, 9741−9748

AUTHOR INFORMATION

Corresponding Author

*Phone: 080-22082298. Fax: 080-22082627. E-mail: sebastiancp@jncasr.ac.in.

Notes

The authors declare no competing financial interest.

ACKNOWLEDGMENTS

We thank the Jawaharlal Nehru Centre for Advanced Scientific Research, Sheikh Saqr Laboratory, and Department of Science and Technology, India (DST), for financial support. S.S. thanks the Council of Scientific and Industrial Research for a research fellowship, and S.C.P. thanks the DST for the Ramanujan fellowship. We are grateful to Prof. C. N. R. Rao for his constant support and encouragement. We thank Prof. A. Gupta and Dr. V. R. Reddy for helping with ^{151}Eu Mössbauer spectroscopic measurements at the UGC-DAE consortium centre at Indore, India. We are thankful to DST and the Saha Institute of Nuclear Physics for funding, DESY, Germany, for the XANES beamline, and Dr. Gerd Wellenreuther for helping with measurements. We also thank Mr. Rana Saha, Mr. Bharat Rajeshwaran, and Mr. Udumula Subbarao for their help in various measurements.

REFERENCES

(1) Aynajian, P.; da Silva Neto, E. H.; Gyenis, A.; Baumbach, R. E.; Thompson, J. D.; Fisk, Z.; Bauer, E. D.; Yazdani, A. *Nature* **2012**, *486*, 201−206.

(2) Custers, J.; Lorenzer, K.-A.; Müller, M.; Prokofiev, A.; Sidorenko, A.; Winkler, H.; Strydom, A. M.; Shimura, Y.; Sakakibara, T.; Yu, R.; Si, Q.; Paschen, S. *Nat. Mater.* **2012**, *11*, 89−94.

(3) Tran, V. H.; Kaczorowski, D.; Khan, R. T.; Bauer, E. *Phys. Rev. B* **2011**, *83*, 064504.

(4) Shim, J. H.; Haule, K.; Kotliar, G. *Science* **2007**, *318*, 1615−1617.

(5) Arora, P.; Chattopadhyay, M. K.; Chandra, L. S. S.; Sharma, V. K.; Roy, S. B. *J. Appl. Phys.* **2012**, *112*, 033906.

(6) Phelan, W. A.; Menard, M. C.; Kangas, M. J.; McCandless, G. T.; Drake, B. L.; Chan, J. Y. *Chem. Mater.* **2012**, *24*, 409−420.

(7) Winkelmann, H.; Elmeguid, M. M. A.; Micklitz, H.; Sanchez, J. P.; Geibel, C.; Steglich, F. *Phys. Rev. Lett.* **1998**, *81*, 4947−4950.

(8) Bianchi, A.; Movshovich, R.; Vekhter, I.; Pagliuso, P. G.; Sarrao, J. L. *Phys. Rev. Lett.* **2003**, *91*, 257001.

(9) Hoffmann, R. D.; Pöttgen, R. *Z. Kristallogr.* **2001**, *216*, 127−145.

(10) Tang, F.; Frontzek, M.; Dshemuchadse, J.; Leisegang, T.; Zschornak, M.; Mietrach, R.; Hoffmann, J. U.; Loser, W.; Gemming, S.; Meyer, D. C.; Loewenhaupt, M. *Phys. Rev. B* **2011**, *84*, 104105.

(11) Gil, R. C.; Carrillo-Cabrera, W.; Schultheiss, M.; Peters, K.; von Schnering, H. G; Grin, Yu. *Z. Anorg. Allg. Chem.* **1999**, *625*, 285−293.

(12) Schnering, H. G. V.; Bolle, U.; Curda, J.; Peters, K.; Carrillo-Cabrera, W.; Somer, M.; Schultheiss, M.; Wedig, U. *Angew. Chem., Int. Ed. Engl.* **1996**, *35*, 984−986.

(13) Xie, Q.; Reyes, E. C.; Wörle, M.; Nesper, R. *Z. Anorg. Allg. Chem.* **2011**, *637*, 846−858.

(14) Gordon, R. A.; Warren, C. J.; Alexander, M. G.; DiSalvo, F. J.; Pöttgen, R. *J. Alloys Compd.* **1997**, *248*, 24−32.

(15) Szlawska, M.; Kaczorowski, D. *Phys. Rev. B* **2011**, *84*, 094430.

(16) Chevalier, B.; Lejay, P.; Etourneau, J. R.; Hagenmuller, P. *Solid State Commun.* **1984**, *49*, 753−760.

(17) Kotsanidis, P. A.; Yakinthos, J. K.; Gamariseale, E. *J. Magn. Magn. Mater.* **1990**, *87*, 199−204.

(18) Majumdar, S.; Sampathkumaran, E. V.; Brando, M.; Hemberger, J.; Loidl, A. *J. Magn. Magn. Mater.* **2001**, *236*, 99−106.

(19) Bärnighausen, H.; Müller, U. *Symmetriebeziehungen zwischen den Raumgruppen als Hilfsmittel zur straffen Darstellung von Strukturzusammenhngen in der Kristallchemie*. Universität Karlsruhe and Universität-Gh Kassel, Germany, 1996.

(20) Bärnighausen, H. *Commun. Math. Chem.* **1980**, *9*, 139−175.

(21) Chevalier, B.; Lejay, P.; Etourneau, J.; Hagenmuller, P. *Solid State Commun.* **1984**, *49*, 753−760.

(22) Rodewald, U. Ch.; Hoffmann, R. -D.; Poettgen, R.; Sampathkumaran, E. V. *Z. Naturforsch. B* **2003**, *58*, 971−974.

(23) Gladyshevskii, R. E.; Cenzual, K.; Parthé, E. *J. Alloys Compd.* **1992**, *189*, 221−228.

(24) Mayer, I.; Felner, I. *J. Solid State Chem.* **1973**, *8*, 355−356.

(25) Shigetoh, K.; Hirata, D.; Avila, M. A.; Takabatake, T. *J. Alloys Compd.* **2005**, *403*, 15−18.

(26) Danzenbacher, S.; Kucherenko, Y.; Vyalikh, D. V.; Holder, M.; Laubschat, C.; Yaresko, A. N.; Krellner, C.; Hossain, Z.; Geibel, C.; Zhou, X. J.; Yang, W. L.; Mannella, N.; Hussain, Z.; Shen, Z. X.; Shi, M.; Patthey, L..; Molodtsov, S. L. *Phys. Rev. B* **2007**, *75*, 045109.

(27) Nishioka, T.; Tabata, Y.; Taniguchi, T.; Miyako, Y. *J. Phys. Soc. Jpn.* **2000**, *69*, 1012−1015.

(28) Patil, S.; Pandey, S. K.; Medicherla, V. R. R.; Singh, R. S.; Bindu, R.; Sampathkumaran, E. V.; Maiti, K. *J. Phys. Condens. Matter* **2010**, *22*, 255602.

(29) Patil, S.; Medicherla, V. R. R.; Singh, R. S.; Pandey, S. K.; Sampathkumaran, E. V.; Maiti, K. *Phys. Rev. B* **2010**, *82*, 104428.

(30) Patil, S.; Iyer, K. K.; Maiti, K.; Sampathkumaran, E. V. *Phys. Rev. B* **2008**, *77*, 094443.

(31) Chondroudi, M.; Peter, S. C.; Malliakas, C. D.; Balasubramanian, M.; Li, Q. A.; Kanatzidis, M. G. *Inorg. Chem.* **2011**, *50*, 1184−1193.

(32) Gaudin, E.; Chevalier, B.; Heying, B.; Rodewald, U. C.; Pöttgen, R. *Chem. Mater.* **2005**, *17*, 2693−2700.

(33) Ivanshin, V. A.; Sukhanov, A. A.; Sokolov, D. A.; Aronson, M. C.; Jia, S.; Bud'ko, S. L.; Canfield, P. C. *J. Alloys Compd.* **2009**, *480*, 126−127.

(34) Kaczorowski, D.; Leithe-Jasper, A.; Rogl, P.; Flandorfer, H.; Cichorek, T.; Petri, R.; Andraka, B. *Phys. Rev. B* **1999**, *60*, 422−433.

(35) Murani, A. P. *NATO Sci. Ser., II: Math.* **2003**, *110*, 297−305.

(36) Peter, S. C.; Sarkar, S.; Kanatzidis, M. G. *Inorg. Chem.* **2012**, *51*, 10793−10799.

(37) Peter, S. C.; Malliakas, C. D.; Chondroudi, M.; Schellenberg, I.; Rayaprol, S.; Hoffmann, R. D.; Pöttgen, R.; Kanatzidis, M. G. *Inorg. Chem.* **2010**, *49*, 9574−9580.

(38) Sheldrick, G. M. *Acta Crystallogr., Sect. A* **2008**, *64*, 112−122.

(39) *SHELXTL 5.10*; Bruker Analytical X-ray Systems, Inc.: Madison, WI, 1998.

(40) Sheldrick, G. M. *SHELXTL, Structure Determination Program*, version 5; Siemens Analytical X-ray Instruments, Inc.: Madison, WI, 1995.

(41) Rodriguez-Carvajal, J. *Physica B* **1993**, *192*, 55−69.

(42) Pöttgen, R. *Z. Naturforsch. B* **1995**, *50*, 1071−1074.

(43) Merlo, F.; Pani, M.; Canepa, F.; Fornasini, M. L. *J. Alloys Compd.* **1996**, *232*, 289−295.

(44) Abicht, H.-P.; Hönle, W.; von Schnering, H. G. *Z. Anorg. Allg. Chem.* **1984**, *519*, 7−23.

(45) Takigawa, Y.; Noguchi, S.; Okuda, K. *J. Magn. Magn. Mater.* **1988**, *76*−*77*, 345−346.

(46) Pagliuso, P. G.; Sarrao, J. L.; Thompson, J. D.; Hundley, M. F. *Phys. Rev. B* **2001**, *63*, 092406.

(47) Bobev, S.; Bauer, E. D.; Thompson, J. D.; Sarrao, J. L.; Miller, G. J.; Eck, B.; Dronskowski, R. *J. Solid State Chem.* **2004**, *177*, 3545−3552.

(48) Pandey, A.; Mazumdar, C.; Ranganathan, R. *J. Phys.: Condens. Matter* **2009**, *21*, 216002.

(49) Emsley, J. *The Elements*; Clarendon Press: Oxford, 1989.

(50) Donohue, J. *The Structures of the Elements*; Wiley: New York, 1974.

(51) Endstra, T.; Nieuwenhuys, G. J.; Mydosh, J. A. *Phys. Rev. B* **1993**, *48*, 9595−9605.

(52) Chevalier, B.; Pöttgen, R.; Darriet, B.; Gravereau, P.; Etourneau, J. *J. Alloys Compd.* **1996**, *233*, 150−160.

(53) Belan, B. D.; Soroka, I. N.; Kryvulya, L. V.; Bodak, O. I.; Protsyk, O. S. *Visn. L'viv. Derzh. Univ. (Ser. Khim.)* **1999**, *38*, 54−57.

(54) Morawiec, H.; Stróż, D.; Goryczka, T.; Chrobak, D. *Scr. Mater.* **1996**, *35*, 485−490.
(55) Ren, X.; Miura, N.; Zhang, J.; Otsuka, K.; Tanaka, K.; Koiwa, K.; Suzuki, T.; Chumlyakov, Yu. I.; Asai, M. *Mater. Sci. Eng., A* **2001**, *312*, 196−206.
(56) Ren, X.; Miura, N.; Otsuka, K.; Suzuki, T.; Tanaka, K.; Chumlyakov, Yu.I.; Asai, M. *Mater. Sci. Eng., A* **1999**, *273*−*275*, 190−194.
(57) Inoue, T.; Kubozono, Y.; Kashino, S.; Takabayashi, Y.; Fujitaka, K.; Hida, M.; Inoue, M.; Kanbara, T.; Emura, S.; Uruga, T. *Chem. Phys. Lett.* **2000**, *316*, 381−386.
(58) Kim, K.-B.; Koo, K.-W.; Cho, T.-Y.; Chun, H.-G. *Mater. Chem. Phys.* **2003**, *80*, 682−689.
(59) Oshio, S.; Matsuoka, T.; Tanaka, S.; Kobayashi, H. *J. Electrochem. Soc.* **1998**, *145*, 3903−3907.
(60) Kim, K.-B.; Kim, Y. I.; Chun, H.-G.; Cho, T.-Y.; Jung, J.-S.; Kang, J. G. *Chem. Mater.* **2002**, *14*, 5045−5052.
(61) Müllmann, R.; Mosel, B. D.; Eckert, H.; Pöttgen, R.; Kremer, R. K. *Hyperfine Interact.* **1997**, *108*, 389−400.